Dimethoxytriazine-Triazole Linked Mesoporous Silica Hybrid Sorbent for Cationic Dyes Adsorption

Ali Saad, Khouloud Jlassi, Manef Abderrabba, Mohamed Chehimi

Dimethoxytriazine-Triazole Linked Mesoporous Silica Hybrid Sorbent for Cationic Dyes Adsorption

Graphical abstract

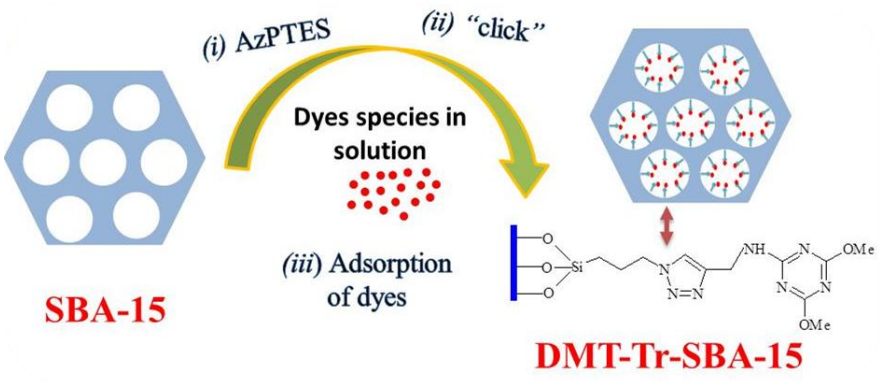

Abstract

Organic dye has always been considered one of the most serious water pollutants. Therefore, the great challenge nowadays is to synthesize effective adsorbents for removal of these contaminants. Herein, we prepared successfully a novel sorbent based on dimethoxy-triazine/triazole groups functionalized via a 1,3-dipolar cycloaddition click reaction on mesoporous silica SBA-15. The resulting sample denoted DMT-Tr-SBA-15 was characterized by FTIR spectra, X-ray photoelectron spectroscopy (XPS), solid-state ^{13}C NMR spectroscopy and nitrogen adsorption/desorption isotherm. The resulting hybrid silica material was applied for the recovery of four cationic dyes in aqueous media. It showed high adsorption efficiency and a fast removal rate. Dye adsorption was monitored versus time; using a 40 mg/L of adsorbent in neutral aqueous solution. The adsorption equilibria were reached within 40 min. The methylene blue adsorption capacity of the functionalized mesoporous silica was found to be 1.848 mmol g^{-1} (591 mg.g^{-1}) at room temperature and pH=7. These results indicate the great potential of clickable mesoporous silica to diversify the active sites for adsorption, thus demonstrating a significant interest for environmental applications.

Keywords: mesoporous SBA-15, triazine/triazole, 1,3-dipolar cycloaddition, adsorption, dye removal.

1. Introduction

Organic dye pollutants have been extensively used for a long time in various industrial fields such as printing, textile, and cosmetics [1]. Some of these dyes can cause various diseases and carcinogenic effects and negative impacts on the environment [2]. To address this concern, many processes have been developed for dyes removal such as; photocatalysis [3, 4], membrane filtration [5], ultrafiltration [6] and adsorption [7,8,9]. Among them, adsorption has emerged as potential, low cost, simple and efficient alternative [10]. Therefore, the synthesis of new convenient adsorbent with high adsorption capacity is extremely significant.

Ordered mesoporous silica (OMS) have large surface area and accessible pore volume [11,12] which make them suitable materials for the efficient adsorption of a wide range of pollutants [13]. However, the mesoporous silica with its surface containing inert silanol groups cannot be used directley without modification [14]. Therefore, organic ligands can be immobilized on mesoporous silica via functionalization of those silanol groups ≡Si-OH [15,16]. To date, several functional groups containing donor atoms (i.e., O/N/S/P) were successfully attached to OMS and used for organic pollutants adsorption and heavy metal extraction, namely: Bis (2 benzimidazolyl)pyridine (bbp) [17], thenoyltrifluoroacetone (TTA) [18], benzene-1,3,5-triamido-tetraphosphonic acid [19], carboxylic acid [20] and phosphoryl functionalized OMS [21].

Among the wide variety of possible reactions for functionalization, copper (I) catalyzed azide−alkyne cycloaddition (CuAAC) click reaction is a common approach to introduce electron-rich heterocycles on mesoporous silica [22,23,24] which received remarkable interest in various fields such as removal of antibiotics [25], catalyst supports [26,27], immobilization of enzymes [28] and biosensing applications [29]. Recently, a huge number of significant researchers on triazole-modified mesoporous silica have been reported in literature as adsorbents (**Table 1**).

Table 1: Recent triazol linked mesoporous silica via azide−alkyne cycloaddition to generate hybrid adsorbents.

N_3-Mesoporous silica	**Grafted molecules**	**Sorbates**	**ref**
N_3-SBA-15	phenylacetylene	Phenols	[30]
N_3-SBA-15	propargylamine propargylsulfone	Niobium and copper species	[31]
N_3-HNS (Hollow nanostructured silica)	1-heptyne 2-butyne-1,4-diol propargyl alcohol phenylacetylene	Antibiotics	[25]
N_3- Silica	10-undecynoic acid	Neutral and acidic drugs	[32]
N_3- SBA-15	3-ethynyl-1-methylimidazole	5-amino-4-hydroxy-7-sulfonaphthalene-2-sulfonate anion (H-acid)	[33]
N_3- SBA-15	propargyl alcohol	Copper	[34]

Electron-rich heterocycles attached to silica surface allow the hybrid material to interact easily with organic dyes by variety of possible adsorption mechanisms such as π–π hydrophobic, electrostatic interaction, van der Waals interactions, hydrogen bonding or coordinative bond that makes them suitable for the adsorption and/or catalytic application [35, 36]. For instance, in our previous work we constructed triazole/triazine-functionalized SBA-15 through CuAAC and subsequently we immobilized the palladium nanoparticles used efficiently for the catalytic reduction of 4- nitrophenol [27]. In this context, Taheri and coworkers [37] reported dendrimer amines based on 1,3,5-triazines modified MCM-48 as efficient silver ions removal from aqueous solution and electroplating industry wastewater.

Taking advantage of the outstanding properties of OMS and electron-rich heterocycles, herein, we selected N-rich linker dimethoxy 1,3,5-triazine complexes as ligands to synthesize a novel hybrid material denoted DMT-Tr-SBA-15. The schematic process to produce the ligand-modified mesoporous silica is displayed in **Figure 1.** The first step consists in the modification of the SBA-15 by an azido-propylsilane. Then in second step the propargyl-4,6-dimethoxy-1,3,5-triazine N-rich ligand was synthesized from 2-Chloro-4,6-dimethoxy-1,3,5-triazine by reaction witch propargylamine. As a third step, we used the conventional click

coupling reaction between azido groups attached to SBA-15 (N_3-SBA-15) and the alkyne group from modified triazine ligand in the presence of copper species as catalyst. Finally, the hybrid material DMT-Tr-SBA-15 was evaluated as adsorbent of four cationic dyes from an aqueous media. The hybrid material showed high adsorption efficiency and rate.

The novelty of our approach lies in the unique use of click chemistry reaction to modify a high surface area pristine material (SBA-15) by different active sites (triazine and triazole moieties) for high adsorption capacity of cationic dyes adsorbates.

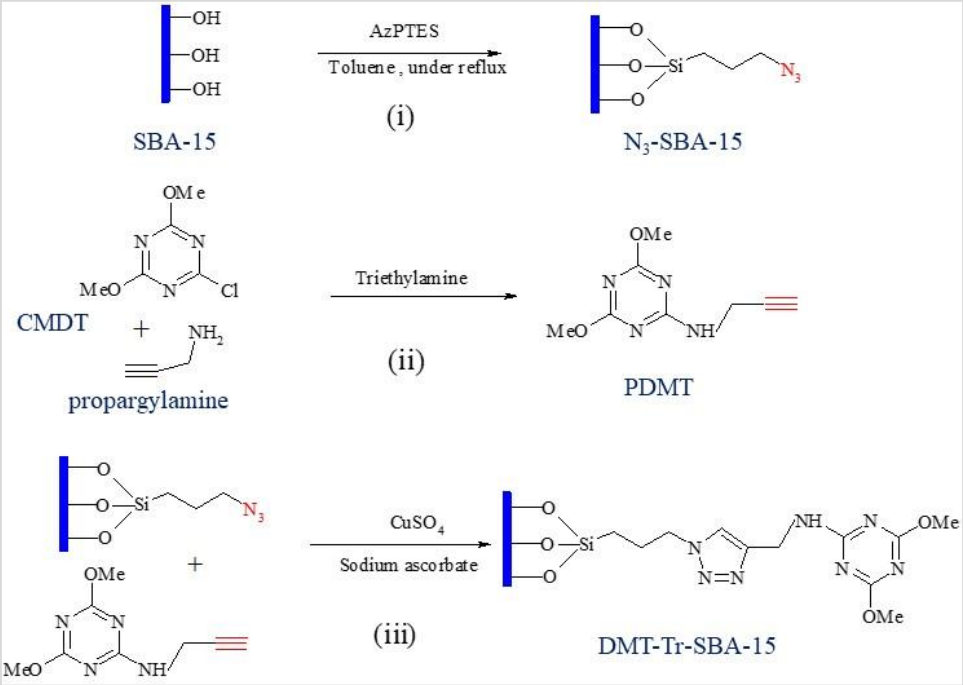

Figure .1. Molecular view of dimethoxytriazine/triazole linked covalent mesoporous silica preparation.

2. Experimental section

2.1. Material

Poly(ethylene oxide)-b-poly(propylene oxide)-b-poly(ethyleneoxide) [$EO_{20}PO_{70}EO_{20}$, Pluronic P123, Mw =5800], tetraethylorthosilicate (TEOS, 98%), propargylamine, 3 chloropropyltriethoxysilane, 2-chloro-4,6-dimethoxy-1,3,5-triazine (CDMT), , acetone, triethylamine, tetrahexylammonium bromide, sodium azide (NaN_3), acetonitrile (ACN), anhydrous pentane, anhydrous toluene, copper sulfate ($CuSO_4$), sodium ascorbate,

dimethylformamide (DMF), HCl, ethanol, and propan-2-ol. Water was deionized using the Milli-Q system of Millipore.

2.2. Synthesis of SBA-15 mesoporous silica

SBA-15 mesoporous silica was prepared along the method previously described by Zhao *et al*. [38]. Briefly, Pluronic P123 was mixed with HCl (3g /16.5 ml); the mixture was diluted using 112 ml of deionized water and stirred for three hours at 40 °C, then TEOS (7.427 g) was added to the mixture. After 2h (at 40 °C) a gel was formed, and the mixture was transferred for condensation at 90 °C for 24 h. Following drying and washing, the organic template was removed by calcination at (550 °C with a heating rate set at 2°C min^{-1}, under air and at set final temperature the solid was left 6h).

2.3. Preparation of dimethoxytriazine/triazole linked covalent mesoporous SBA-15

2.3.1. Synthesis of the azidopropyltriethoxysilane-functionalized SBA-15

The used 3-azidopropyltriethoxysilane coupling agent (AZPTES) was fabricated as described in [39]. The as prepared silane (AZPTES) was colorless liquid. ^{1}H NMR ($CDCl_3$): δ (ppm) = 3.75 (q, 6 H; CH_3CH_2O), 3.20 (t, 2H; CH_2N_3), 1.64 (m, 2H; $SiCH_2CH_2$), 1.16 (t, 9H, CH_3CH_2O), 0.61 (m, 2H; $SiCH_2$) (see Figure S1). Functionalization was performed by dispersing 1g of SBA-15 in 50 mL of toluene, then 1.96 g of AZPTES were added under nitrogen atmosphere, and subsequently the mixture was stirred for 24 h at 80 °C. After the completion of reaction, the mixture was cooled, filtered and washed with toluene and ethanol.

2.3.2 Synthesis of 2-Propargy-4, 6-dimethoxy-1, 3, 5-triazine (PDMT)

Firstly, (1.2 g, 6.9 mmol) of 2-Chloro-4,6-dimethoxy-1,3,5-triazine was added to a mixture of propargylamine (0.45 g, 8.2 mmol) and triethylamine (0.57 g, 6.9 mmol) in 120 mL acetone. The solution was then heated, filtered, then dried under vacuum. The final isolated product is a white powder. ^{1}H NMR ($CDCl_3$, 400 MHz): δ (ppm) = 5.7 (H, N-H); δ (ppm) = 4.15 (dd, 2H, N-CH_2-C); δ (ppm) = 3.9 (d, 6H, O-CH_3); 2.2(t, H, alkyne C-H) (see Figure S2).

2.3.3 Preparation of DMT-Tr-SBA-15

4, 6-dimethoxy 1,2,3-Triazole -1,3,5-Triazine (DMT-Tr) ligand decorated SBA-15 was obtained by 1,3-dipolar cycloaddition reactions. First, 1.22 g of N_3-SBA-15, 0.43g of CuSO4

(0.1M), and 0.77 g of sodium ascorbate solution (0.1M) was added to a solution of 2-propargy-4,6-dimethoxy-1,3,5-triazine (0.47g, 1M) in 50% aqueous propan-2-ol (20 ml). The obtained mixture was maintained under stirring for 24 h at room temperature. After filtration, washing and vacuum drying, the final product was isolated and abbreviated DMT-Tr-SBA-15.

2.4. Adsorption experiments

30 mg of the adsorbent DMT-Tr-SBA-15 were dispersed in 500 mL of aqueous organic dye solution and the mixture was stirred at 300 rpm, at 25°C for a predefined period of time. After reaching equilibrium time, the mixture filtered using membrane filter to separate the solid and liquid phases. The dye concentration in the filtrate was determined by UV-Vis spectrophotometry at the maximum absorbance of each dye. The removal percentage of each dye was calculated as follows:

$$R\,\% = \left[\frac{C_0 - C_{eq}}{C_0}\right] x\ 100 \qquad (1)$$

where C_0 and C_{eq} are the initial and equilibrium concentration of organic dye ($mg.L^{-1}$), respectively. The amount of each dye adsorbed onto DMT-Tr-SBA-15 (q_t) was calculated using:

$$q_t = [\frac{(C_0 - C_t)x\ V}{m}] \qquad (2)$$

where q_t is the amount of dye adsorbed and C_t is the dye concentration in the solution at time t and m amount of sorbent (g).

The adsorption capacity expressed in mmol/g was calculated as follows:

$$q_e(mmol/g) = \frac{q_e(mg/g)}{M(g/mol-1)}] \qquad (3)$$

2.5. Characterization

The ^{1}H, and ^{13}C MAS NMR spectra were acquired, using Bruker AVANCE 300 wide bore spectrometer using deuterated chloroform as the solvent and internal standard. Fourier transform infrared (FTIR) spectra were recorded using an EQUINOX 55 (Bruker) spectrometer ranging from 4000 to 400 cm^{-1}. X-ray photoelectron spectroscopy (XPS)

measurements were made using a K Alpha (Thermo) fitted with a monochromatic Al K X-ray source (spot size: 400 µm). The spectra were calibrated against the C1s component set at 284.9 eV. Thermogravimetric analyses were performed using a SETSYS evolution 16 apparatus from SETARAM by heating up the sample from room temperature up to 800°C under air flow (55 cm^3 (STP)/min) with a heating rate of 10 °C min^{-1}. Nitrogen adsorption and desorption studies were carried using an autosorb IQ Quantachrome. The specific surface (S_{BET}) values were obtained using the Brunauer-Emmett-Teller (BET) method, [40] while the mesopore size study of the materials was carried out using the Barrett-Joyner-Halenda (BJH) method [41].

3. Results and discussion

3.1. Physicochemical properties of materials.

3.1.1. Fourier transform infrared spectroscopic analysis.

The dimethoxy-triazine ligand FT-IR changes upon modification are presented in **Figure 2a**. The spectrum of pure 2-chloro-4,6-dimethoxy-1,3,5-triazine (CDMT) exhibits the characteristic absorption bands in the 478–1662 cm^{-1} range *i.e.* 1562, 1460, 1300, 818 and 558 cm^{-1} that can be assigned to aromatic stretching modes in triazine ring, C=N, C−O stretching, C−N stretching, and C−H outer-bending vibrations, respectively. After reaction with propargylamine, the characteristic bands of the triazine ring appear. The new peaks centred at at 2109, 2923, 2961, 3128 and 3244 cm^{-1}, can be assigned to the triple bond C≡C, ν_{sy} CH in (-CH_2 – group), ν_{as} CH (in -CH_2 – group), N-H secondary amine and the C-H stretch on the terminal alkyne, respectively.

Figure 2b shows the synthesis of (3-azidopropyl) triethoxysilane from 3-chloropropyltriethoxysilane. One can clearly observe that after modification, a new peak appears at 2095 cm^{-1}; it can be ascribed to the azido groups [25,42].

Figure 2c shows the spectra of SBA-15-based materials. All samples exhibited a band at 960 cm^{-1} is a characteristic peak of asymmetric stretching vibrations Si-O-Si [43]. The associated Si−O−Si bands are observed at 1274, 1050, 910, 797, and 448 cm^{-1} [39]. After azido-silanization, an obvious band at 2110 cm^{-1} is observed and assigned to the characteristic stretching vibration of organic azides [25]. After the click reaction, the intensity of the adsorption peak corresponding to the azido group decreases significantly and disappears. New bands are observed in the spectrum of DMT-Tr-SBA-15 between 1589 and 1376 cm^{-1} which can be assigned to ring stretching vibration of conjugated C=C, C=N and C–N in triazine and triazole rings, giving evidence of the successful functionalization of the OMS pristine.

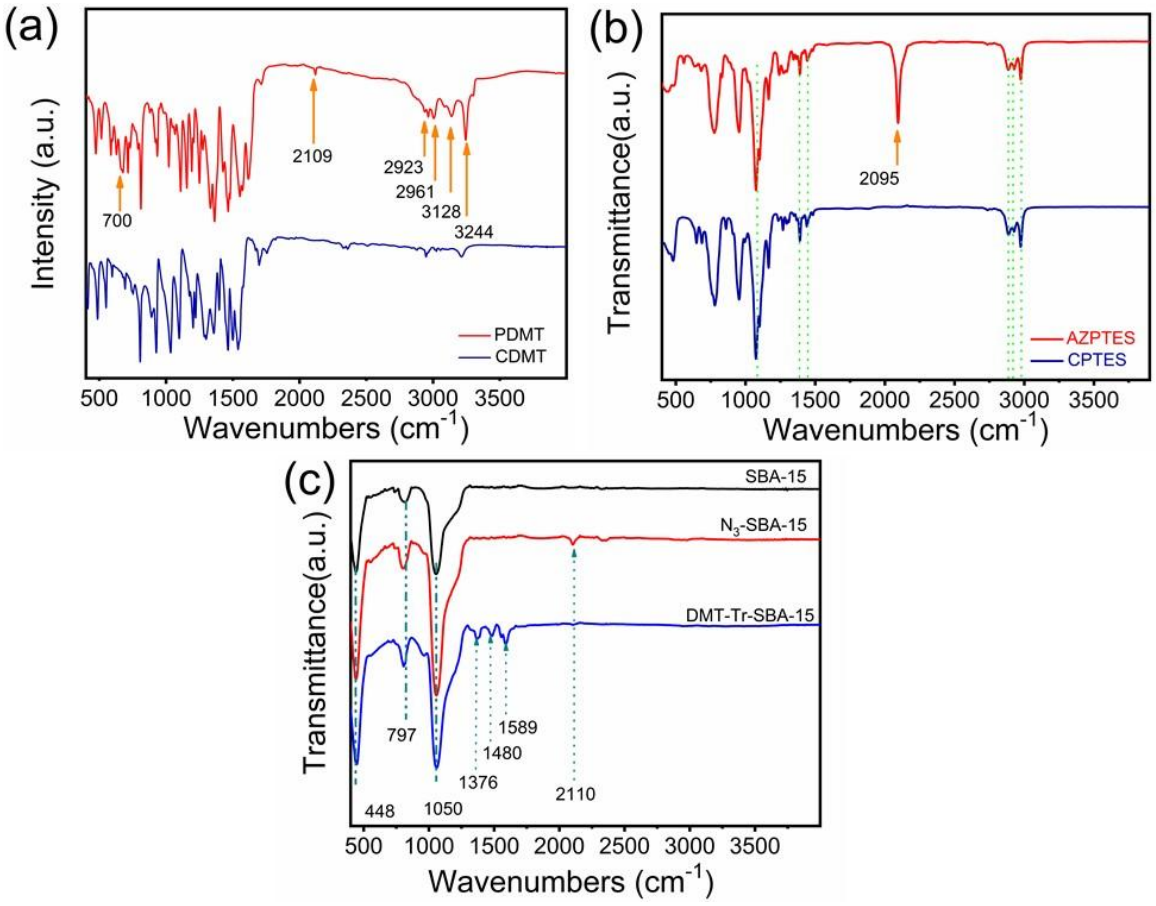

Figure.2. FT-IR spectra of: (a) dimethoxy-triazine ligand before and after modification with propargylamine, (b) (3-azidopropyl)triethoxysilane (AZPTES) and 3-chloropropyltriethoxysilane (CPTES), and (c) SBA-15-based materials.

3.1.2. ^{13}C solid-state NMR analysis

To confirm FTIR studies above, we have employed the Solid-state ^{13}C CP/MAS NMR. Experimental conditions were as follow: contact time of 2 ms and a spinning rate of 10 kHz. NMR spectra of N_3-SBA-15 and DMT-Tr-SBA-15 are displayed in Figure.3. N_3-SBA-15 spectra show three peaks at δ= 9.4, 22.5 and 54 ppm can be attributed to the first carbon (C1) attached to Si, the middle carbon (C2) and the third carbon (C3) attached to the azido groups, respectively **[**44**]**. One can note the presence of two additional peaks signals can be associated to residual P123 template and EtO-groups (59 and 17 ppm) [45]. However, after azide−alkyne modification, extra newly peaks are clearly observed at δ= 120, 145, 165 and 170 ppm, which corresponds to the carbons present in the rings of triazole/triazine attached to the surface. The appearance of smaller peak at 37 ppm in the ^{13}C NMR spectrum of DMT-Tr-SBA-15 corresponds to carbon attached to the oxygen atom in the methoxy group of triazine heterocycles.

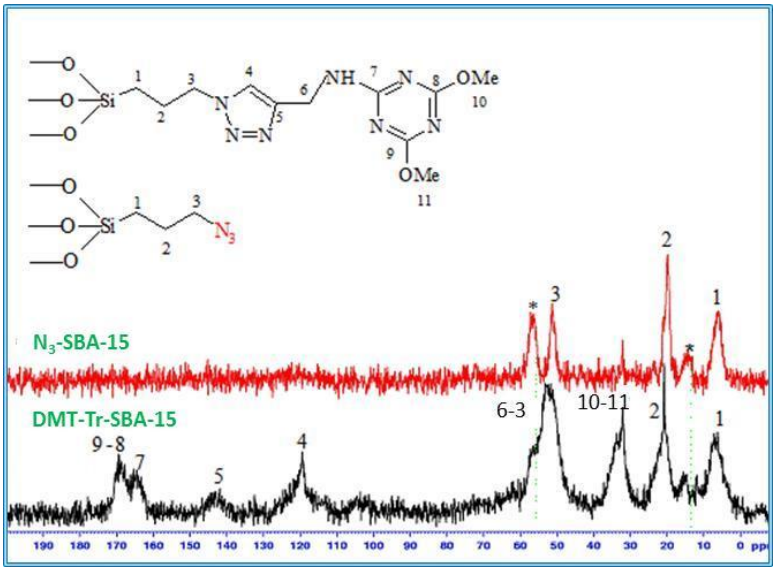

Figure.3. Solid-state ^{13}C CP/MAS NMR spectra of N_3-SBA-15 and DMT-Tr- SBA-15.*Surfactant signals (P123).

3.1.3. X-ray Photoelectron Spectroscopy Surface Analysis.

XPS was used to monitor the stepwise modification of surface chemical composition of the mesoporous silica adsorbent. Survey spectra of pristine and modified mesoporous silica are

shown in Figure. 4. In addition to Si2p (~105 eV), Si2s (~155 eV) and O1s (~532 eV), SBA-15 exhibits a very low intensity C1s peak due to adventitious hydrocarbon contamination. After chemical reaction with AzPTES the survey spectrum shows the appearance of the N1s feature centered at ~399 eV it is strong supporting evidence of the attachment of azidopropyl groups onto surface. This is accompanied by an attenuation of Si2p and Si2s peaks. After CuAAC reaction, C and N contents increase drastically for DMT-TrSBA-15 adsorbent, which accounts for the attachment of the triazine ring to the azido-functionalized silica via 1,3-Huisgen cycloaddition (Table S1, Supporting Information). This modification is noted for the surface, which is important for the interaction with dyes. However, it would also be interesting to determine the total nitrogen loading to silica by elemental analysis [46] and to compare surface and bulk compositions of the DMT-TrSBA-15 adsorbent.

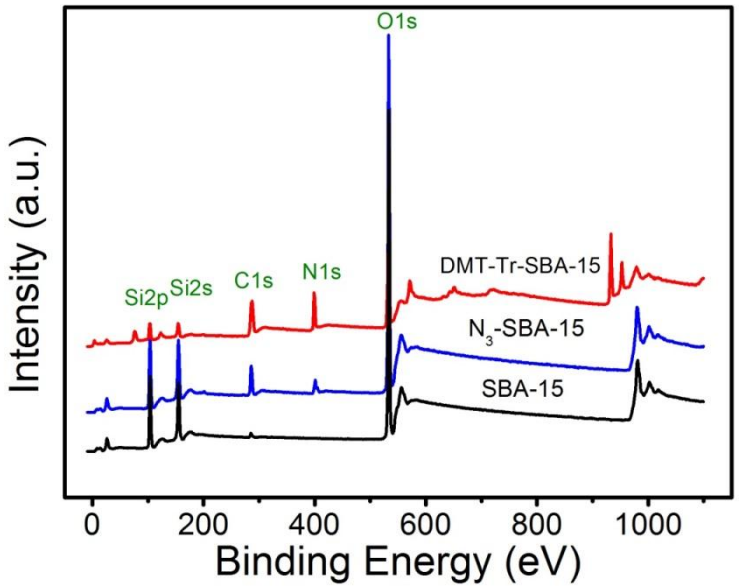

Figure. 4. XPS survey spectra for different SBA-15 materials.

C1s and N1s high resolution regions before and after azide−alkyne 1,3-dipolar cycloaddition are shown in Figure 5. The C1s high resolution XPS spectrum from N_3-SBA-15 (Figure 5a) is fitted with three components assigned to C-C/C-H, N-C and O–C=O carbon environments and centered at 284.9, 286.7 and 288.7 eV, respectively. The high binding energy component O–C=O could originate from SBA-15; this component is invariably detected at the surface of high energy materials such as metals, metal oxides and ceramics [47]. After click reaction, for DMT-Tr-SBA-15, the peak-fitted C1s spectrum of DMT-Tr-SBA-15 (Figure. 5c) shows three peaks at the binding energy values 288.3, 286.3, and 284.2 eV; they can be attributed to

N=C/C=C, N-C/CO and C-C/C-H chemical environments, respectively. A relative increase in the peak component intensity of peaks related to nitrogen (N=C/C=C, N-C/CO) accounts for the presence of triazole and triazine rings at the surface.

The N1s of N_3-SBA-15 (Figure 5b) was fitted in three components; assigned to quaternized –C-N=$\underline{N}^+$=N^- (~404.5 eV), -$\underline{N}$=N^+=$\underline{N}^-$ /N-C (~401 eV) and N−H/N−C (399−400 eV) [27]. The positively charged nitrogen from the azido group coexists in —N=N^+=N^-↔ —N^-—N^+ ≡N mesomeric structures [48]. The main peak centered at ~401 is due to the two other nitrogen atoms which can be negatively charged (see mesomeric structures). After the click reaction, the azide is transformed into triazole and the N^+ peak component, disappeared indicating the successful reaction. The surface analysis results are in line with the FTIR findings which showed the disappearance of the peak related to the organic azides attached to the surface (Figure 2). The sp^3 nitrogen atom has two peaks located at 401.1 eV ascribed to NH^+ groups and/or triazole N^+ atoms respectively. The N=N atoms have a single component centered at 399.8 eV. The first peak at 398.9 eV is assigned to N=C bonds in triazole and triazine rings.

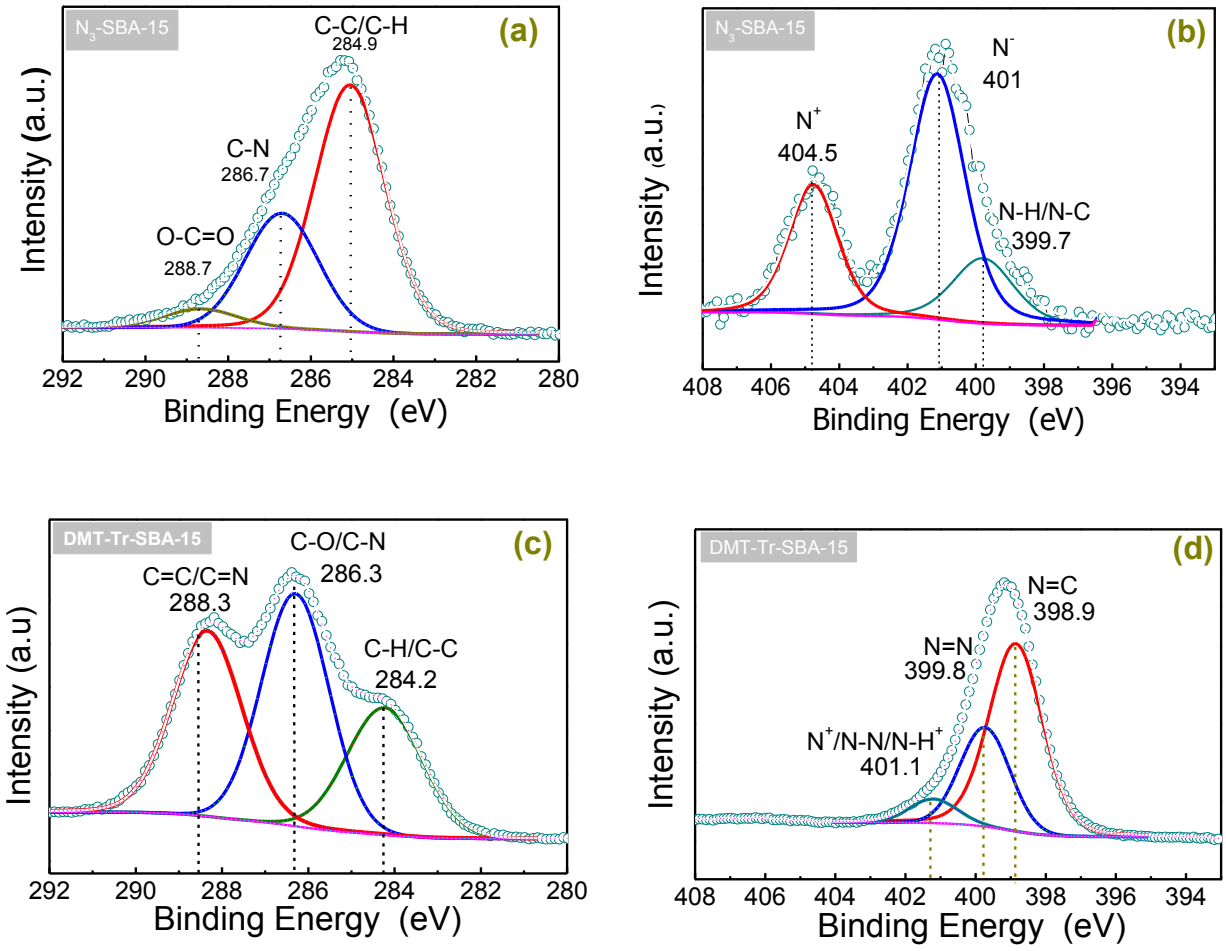

Figure 5. Peak-fitted C1s and N1s regions from N_3-SBA-15 (a, b), and DMT-Tr-SBA-15 (c, d).

3.1.4. Thermal Analysis.

Further to confirm the successful modification, of OMS with the functional groups, thermal stability of all the synthesized materials was studied by thermogravimetric analysis (TGA) under N_2 atmosphere from room temperature to 800 °C under a rate of 10 °C min^{-1}. The plots of pristine are also reported which does not show any significant weight loss due to its higher thermal stability imparted by the strong Si-O-Si bonds. As shown in Figure 6 the first weight loss stage below 190°C correlated to adsorbed physical water, with a total weight loss of 2.06% and 6.95 % for N_3-SBA-15 and DMT-Tr-SBA-15, respectively. Above 250°C a massive thermal decomposition is observed for N_3-SBA-15 and DMT-Tr-SBA-15 with a total

weight loss of 13.5% and 24.6%, respectively. The second weight loss is due to decomposition of the residual surfactant for the pristine and decomposition of the functional groups decorated the OMS network**.** It is important to note that the weight loss difference between N_3-SBA-15 and DMT-Tr-SBA-15 is about 11.1% which is an indication of substantial anchoring of triazole/triazine rings to the mesoporous silica surface.

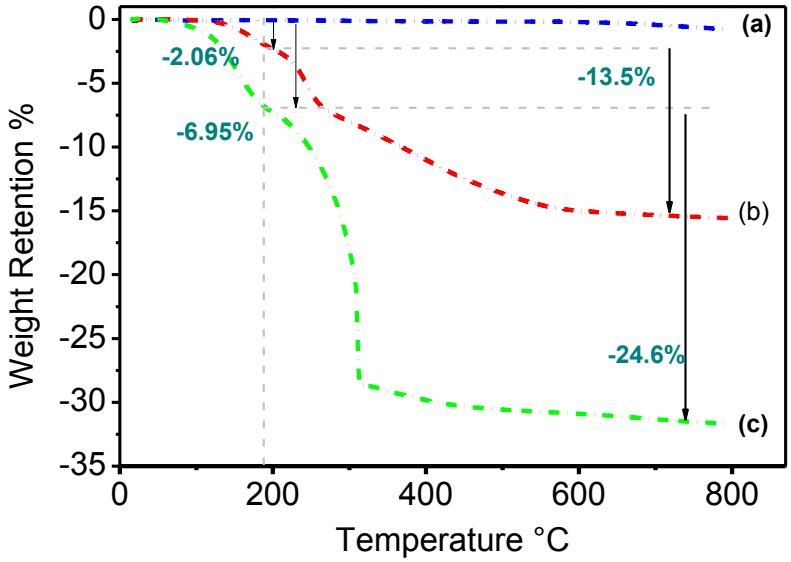

Figure. 6. Thermogravimetric analysis of (a) pristine mesoporous silica SBA-15, (b) N_3-SBA-15, and (c) DMT-Tr-SBA-15

3.1.5. Nitrogen adsorption−desorption isotherms.

To further investigate the textural characteristics of the as-prepared samples N_2 adsorption–desorption isotherms were measured and displayed Figure. 7. The isotherms indicate that our samples display a type-IV sorption isotherm with a sharp inflection step at P/P_0 ranging from 0.55 to 0.75 typical for OMS [49]. The pore-size distribution, is shown as inset the Figure7. The specific surface area, total pore volume, and pore size summarized in Table 2. The pristine OMS display a specific surface area (S_{BET}) around 733.8 m^2g^{-1}, an average pore size (D_p^{BJH}) about 6.81 nm and a pore volume (V_p) about1.15 $cm^3\ g^{-1}$. After azido-silanization, S_{BET}, the V_p and D_p^{BJH} decreased to 375.1g^{-1}, 0.529 $cm^3\ g^{-1}$ and 5.83 nm, respectively. The decrease in S_{BET} is exacerbated after cycloaddition reaction to 276.9 m^2g^{-1}, the D_p^{BJH} was decreased to 5.06 nm, and the V_p was decreased to 0.367 $cm^3\ g^{-1}$. This noteworthy decrease in porosity, S_{BET}, and V_p is, may be caused by the partial blockage of the pores, after the grafting of organic groups on SBA-15 inner walls [50]. This in line with previous publications, for

instance Badiei *et al*. [17] reported the decrease of an initial porosity of 7.1 to 5.7 nm after modification with chloropropyltriethoxysilane then to 4.4 nm after modification with 2,6-bis(2-benzimidazolyl) pyridine in second step.

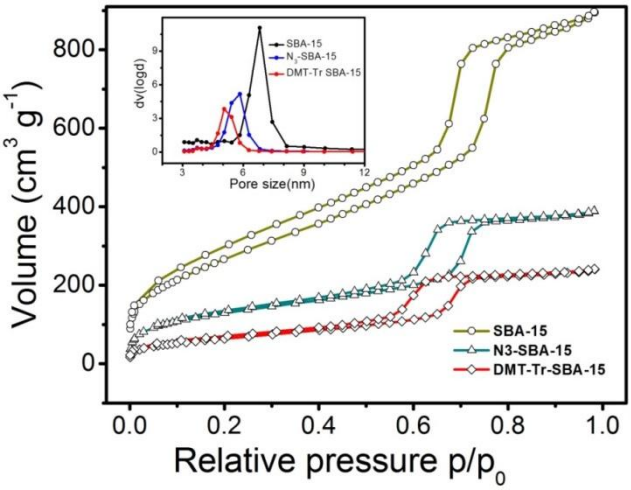

Figure.7. Nitrogen sorption isotherms at 77 K for the N_3-SBA-15, and DMT-Tr-SBA-15 samples.

Table 2 Summary of Nitrogen Sorption Results.

Material	S_{BET} (m^2g^{-1})	D_p^{BJH} (nm)[a]	V_p (cm^3g^{-1})[b]
SBA-15	733.8	6.81	1.15
N_3-SBA-15	375.1	5.83	0.529
DMT-Tr-SBA-15	276.9	5.06	0.367

[a]Mean pore diameter determined using the BJH method

[b]Total pore volume determined at $P/P^0 = 0.97$

3.2. Adsorption of selected cationic dyes

Four cationic dyes; namely rhodamine B (Rhd B), rhodamine 6G (Rhd 6G), methylene blue (MB), and methyl orange (MO); were employed as adsorbates in order to investigate the adsorption capacity of the DMT-Tr-SBA-15 hybrid material and its potential selectivity

towards one of these dyes. Their molecular structures and chemical properties are reported in Table 2. A series of batch adsorption experiment were carried out at room temperature, using the same amount of the adsorbent (30 mg) and in a neutral aqueous solution. For instance, the normalized concentration curve of methylene blue in the liquid phase and solid phase versus contact time with an initial concentration of 40 mg/L and in neutral solution are plotted in Figure.8a. It can be noticing that at the initial adsorption stage, the adsorbent surface contains a lot of available active sites to adsorbate concentration in the liquid phase which led to a significantly increase of the capacity of adsorption q_{eq}. This result is accompanied by a considerable decrease of the intensity of the maximum UV absorption wavelength as displayed Figure 8b. Consequently, a significant evolution of the color of the aqueous solution for both of MB and Rhd B dyes (inset Figure 8a- and Figure S3 supporting information). In the second adsorption stage, it can be seen after 12 min that the evolution of the capacity of adsorption became slowly till reaching the equilibrium time. This could be due to: (i) a decrease of the dye concentration in liquid phase, (ii) a beginning of the saturation of the available adsorption sites in solid phase, (iii) a combination of these factors [51]. On the other hand, the adsorption rate decreased gradually with increasing contact time and a maximum adsorption of MB was achieved 1.848 mmol g^{-1} at 24 h. Therefore, the minimum contact time of 40 min could be considered for an optimum adsorption of methylene blue.

Table 2. Chemical properties of selected dyes.

Dye	M.W.	UV absorption wavelength (nm)	Type	Molecular structure
MB 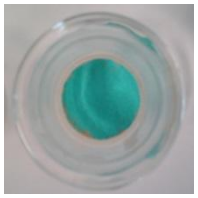	319.85	664	Cationic dye	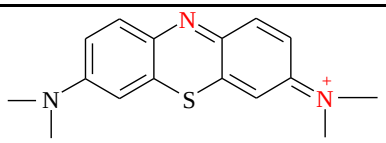
Rhd B 	479.01	551	Cationic dye	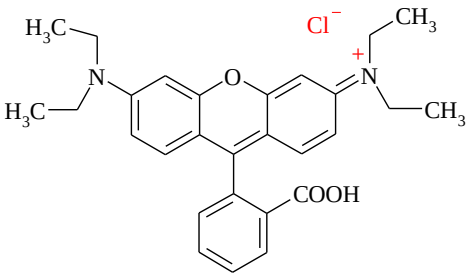
Rhd 6G 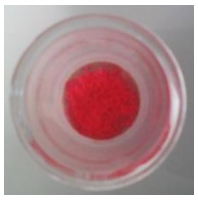	479.01	496	Cationic dye	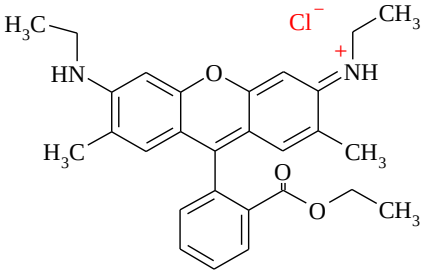
MO 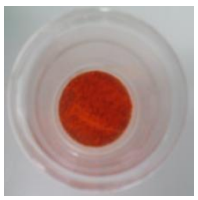	305.35	466	Cationic dye	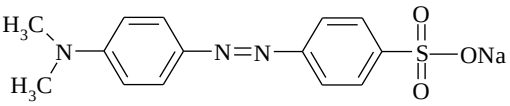

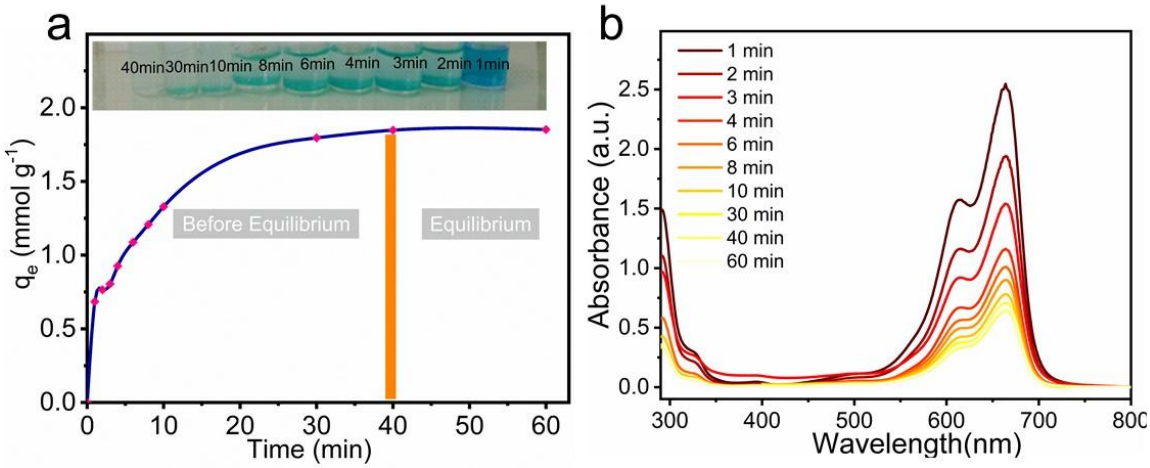

Figure 8. (a) Equilibrium adsorption isotherm of MB onto the DMT-Tr-SBA-15 at 25°C; inset shows optical images of dyes solutions MB with the DMT-Tr-SBA-15 adsorbent. (b) Temporal evolution of UV-Vis absorption spectra of MB.

In order to study the selectivity of the DMT-Tr-SBA-15 toward the adsorption of these cationic dyes, Figure 9 display the removal efficiency histograms and adsorption capacity of all of selected dyes in the same conditions (30 mg mass of the adsorbent, 40 min as equilibrium time and initial dye concentration: 40 mg/L). The capacity of adsorption q_{eq} of for MB, Rdh B, Rdh 6G and MO at the equilibrium time is 1.848, 1.036, 0.952, and 1.606 mmol.g^{-1}, respectively. Based on the q_{eq} results, it is clear that the novel adsorbent presents a good removal efficient (74 % for Rhd B, 68% for Rhd 6G, 73% for MO, and 88% for MB) and excellent adsorption capacity for all of selected dyes can be attributed to the surface-active sites for adsorption. The adsorption capacity of DMT-Tr-SBA- follows the sequence MB > MO> Rhd B> Rhd 6G. The higher removal efficient for MB adsorbates could be explained by the favored/strong interactions of its positive functional groups and the high density of negative active sites onto adsorbent surface.

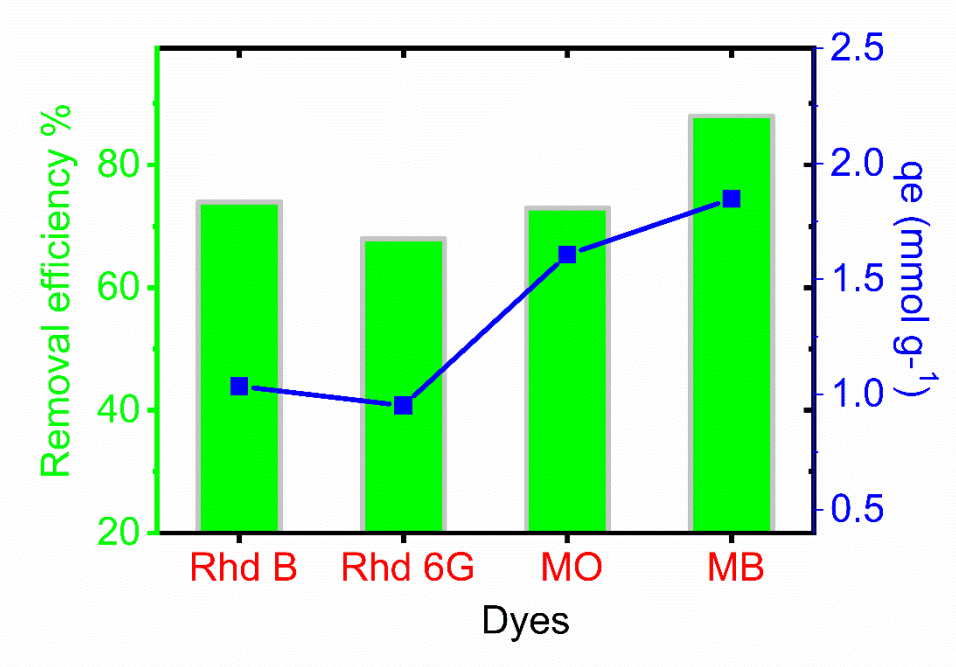

Figure. 9. Removal efficiency of selected dyes by the DMT-Tr-SBA-15 adsorbent (30 mg) at room temperature, after optimum contact time and initial dye concentration of 40 mg/L.

In the light of the achieved results, it is clear that the DMT-Tr-SBA-15 has excellent capacity and efficiency for cationic dyes adsorption compared to other mesoporous silica-based adsorbents reported in the literature (see Table 3), with a maximum adsorption capacity of 1.848 mmol.g^{-1}, corresponding to 591 mg.g^{-1}, at neutral pH and reached within 40 min. It would be interesting to conduct additional studies in order to determine adsorption isotherm model and apparent adsorption kinetic constant [52].

Table 3. Comparison of the maximum uptake capacity (q_{max}) values of MB in the present study and of other adsorbents reported in literature.

Adsorbent	Maximum adsorption capacity q_{max} (mmol.g^{-1})	pH	Equilibrium time (min)	Reference
β-Cyclodextrin -SBA-15	5.61	-	25	[53]
SBA-15	1.19	8.0	-	[54]
Poly(GDMA)/ MCM-41	0.35	7.0	20 min	[55]
MCM-41	0.206	7.0	60 min	[56]
CuO/MCM-41	0.27	7.0	60 min	[56]
COOH-SBA-16	1.85	9.0	200 min	20
DMT-Tr-SBA-15	1.848	7.0	40 min	This work

Figure 10 displays the chemical structure of the adsorbent. It accounts for the possible molecular interactions with the cationic dyes. Triazine could be protonated and interact with -COO^- group from Rhd B or $–SO_3^-$ from MO. In addition, the cationic sites S^+ in MB and N^+ in Rhd 6G and Rhd B **[**57] favor adsorption on the surface which has silanol groups that are known to deprotonate at pH ~2 to yield SiO^-. Indeed, these dye molecules are completely ionized and become positively charged in the solution. Moreover, DMT-Tr-SBA-15 adsorbent favorably captures aromatic organic molecules via π−π interactions on top of electrostatic, anion−cation interactions **[**58]. MB is smaller and flat dye; it could interact favorably with the triazine and triazole groups via π stacking in addition to H-bonding. Rhd 6G and Rhd B bear ethyl groups (MB has methyl groups) which limit specific interactions and thus account for weak London interactions, hence the lower adsorption capacity for these Rhodamine type dyes compared to MO and particularly MB.

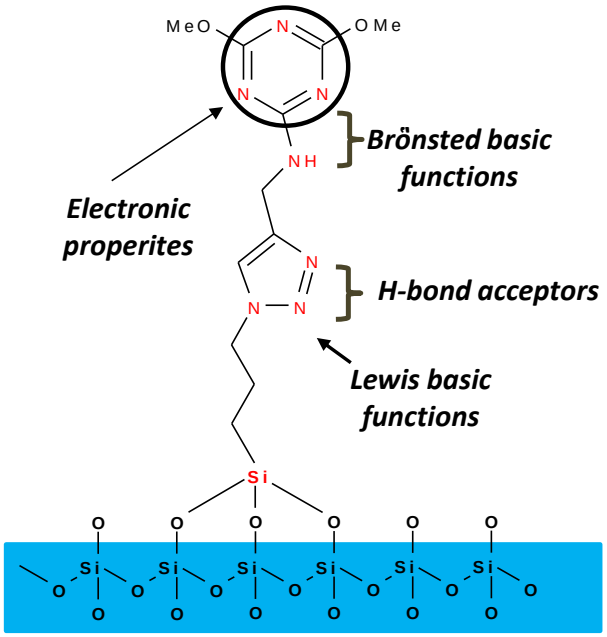

Figure. 10. Schematic illustration of the available adsorption sites onto the DMT-Tr-SBA-15 adsorbent.

Conclusion

To sum up, a novel dimethoxytriazine/triazole linked SBA-15 has been synthetized by CuAAC click reaction. Azido-silanization was conducted in order to achieve silica–heterocycles interface with excellent adhesion. An arsenal of techniques (FTIR spectroscopy, XPS, TGA, ^{13}C solid-state NMR N_2 and sorption measurement isotherms) was employed for structural characterization of the hybrid material. Given the strong electrostatic attraction between its negative surface and cationic charges of adsorbates, this novel hybrid was evaluated to remove four selected cationic dyes from aqueous media. The new hybrid material showed high adsorption efficiency, over 88% for MB and a fast removal rate. The adsorption was monitored versus time; the equilibrium was reached within 40 min for a concentration of 40 mg/L. The maximum adsorption capacity for methylene blue at room temperature and pH 7 was 1.848 mmol.g^{-1} (591 mg.g^{-1}) So far, adsorption of four cationic dyes, with distinct chemical structures, was investigated, one could thus anticipate the DMT-Tr-SBA-15 adsorbent to be efficient for numerous organic dyes.

Acknowledgements
AS wishes to thank the Tunisian Ministry of Higher Education and Scientific Research for the provision of travel grants to conduct research at ITODYS (Université de Paris) and ICMPE (CNRS) research labs.

Declaration of interest: the authors declare no conflict of interest.

References

[1] Han X, Wang Y, Zhang N, Meng J, Li Y, Liang J (2021) Facile synthesis of mesoporous silica derived from iron ore tailings for efficient adsorption of methylene blue. Colloids Surf. A Physicochem. Eng. Asp *617* :126391.

[2] Boukoussa B, Mokhtar A, El Guerdaoui A, Hachemaoui M, Ouachtak H, Abdelkrim S, Addi AA, Babou S, Boudina B, Bengueddach A, Hamacha R (2021) Adsorption behavior of cationic dye on mesoporous silica SBA-15 carried by calcium alginate beads: Experimental and molecular dynamics study. J. Mol. Liq *333* : 115976.

[3] Sunkara JR. Botsa SM (2019) SnO_2/Fe_2O_3/Ag nanocomposite via hydrothermal approach: a novel highly Efficient photodegradation of eosin yellow and brilliant green dyes under Visible light irradiation. Chem. Afr. 2 :635-644

[4]Ouanji F, Ellouzi I, Kacimi M, Ziyad M (2019) Ca-hydroxyzincate: synthesis and enhanced photocatalytic activity for the degradation of methylene blue under UV-light irradiation. Chem. Afr. 2:395-400.

[5] Hea J, Cuia A, Denga S, Chenb JP (2018) Treatment of methylene blue simulated wastewater by a cost-effective microscale biochar/polysulfone mixed matrix hollow fiber membrane: performance and mechanism studies. J. Colloid Interface Sci. 512:190-197.

[6] Parakala S, Moulik S, Sridhar S (2019) Effective separation of methylene blue dye from aqueous solutions by integration of micellar enhanced ultrafiltration with vacuum membrane distillation, Chem. Eng. J 375 :122015.

[7] Afshari M, Dinari M (2020) Synthesis of new imine-linked covalent organic framework as high efficient absorbent and monitoring the removal of direct fast scarlet 4BS textile dye based on mobile phone colorimetric platform. J. Hazard. Mater 385:121514.

[8] Baig MM, Zulfiqar S, Yousuf MA, Shakir I, Aboud MFA, Warsi MF (2021) $DyxMnFe_{2-x}O_4$ nanoparticles decorated over mesoporous silica for environmental remediation applications. J. Hazard. Mater 402:123526.

[9] Teymoorian T, Hashemi N, Mousazadeh MH, Entezarian ZN (2021) S doped carbon quantum dots inside mesoporous silica for effective adsorption of methylene blue dye. SN Applied Sciences 3 :1-14.

[10] Beagan AM (2021) Investigating Methylene Blue Removal from Aqueous Solution by Cysteine-Functionalized Mesoporous Silica. *J. Chem.*

[11]Saad A, Cabet E, Lilienbaum A, Hamadi S, Abderrabba M, Chehimi MM(2017) Polypyrrole/Ag/mesoporous silica nanocomposite particles: Design by photopolymerization in aqueous medium and antibacterial activity, J Taiwan Inst Chem Eng 80:1022-1030.

[12]Saad A, Bakas I, Piquemal JY, Nowak S, Abderrabba M, Chehimi MM (2016) Mesoporous silica/polyacrylamide composite: Preparation by UV-graft photopolymerization, characterization and use as Hg (II) adsorbent. Appl. Surf. Sci 367:181-189.

[13] Czepa W, Pakulski D, Witomska S, Patroniak V, Ciesielski A, Samorì P (2020) Graphene oxide-mesoporous SiO_2 hybrid composite for fast and efficient removal of organic cationic contaminants. Carbon158:193-201.

[14] Ferré M, Pleixats R, Man MWC, Cattoën X (2016) Recyclable organocatalysts based on hybrid silicas, Green Chem 18: 881-922.

[15] El-Nahhal IM, Kodeh FS, Salem JK, Hammad T, Kuhn S, Hempelmann R, Al Bhaisi S (2019) Silica, Mesoporous Silica and Its Thiol Functionalized Silica Coated MgO and Mg(OH)2 Materials. Chem. Afr. 2, 267–276.

[16] Kodeh FS., El-Nahhal IM (2021) Exploring of Potential Antibacterial Activity of Hypochlorite and Chloroamine Adsorbed Ammonium Functionalized Mesoporous SBA-15 Silica. Chem. Afr. 4: 599–605.

[17] Badiei A, Razavi BV, Goldooz H, Ziarani GM, Faridbod F, Ganjali MR (2018) Novel fluorescent chemosensor acssembled with 2,6-Bis(2- Benzimidazolyl)Pyridine functionalized nanoporous silica-type SBA- 15 for recognition of Hg^{2+} Ion in aqueous media. Int. J. Environ. Res. 12:109-115.

[18]Gök M, Sert Ş, Özevci G, Eral M (2018) Efficient adsorption of Th(IV) from aqueous solution by modified SBA-15 mesoporous silica.Nucl Sci Tech. 29 : 95-102.

[19] Ravi S, Lee YR, Yu K, Ahn JW, Ahn WS (2018) Benzene triamido-tetraphosphonic acid immobilized on mesoporous silica for adsorption of Nd^{3+} ions in aqueous solution. Micropor Mesopor Mater 258: 62-71.

[20]Tsai CH, Chang WC, Saikia D, Wu CE, Kao HM (2016) Functionalization of cubic mesoporous silica SBA-16 with carboxylic acid via one-pot synthesis route for effective removal of cationic dyes. J. Hazard. Mater. 309 :236-248.

[21]Xue G, Yurun F, Li M, Dezhi G, Jie J, Jincheng Y, Haibin S, Hongyu G, Yujun Z (2017) Phosphoryl functionalized mesoporous silica for uranium adsorption. Appl. Surf. Sci: 402, 53-60.

[22]Arslan M, Tasdelen MA (2018) Click chemistry in macromolecular design: complex architectures from functional polymers, Chem. Afr. 1:20.

[23] Ziarani GM, Hassanzadeh Z, Gholamzadeh P, Asadi S, Badiei A (2016) Advances in click chemistry for silica-based material construction. RSC Adv 6: 21979-22006.

[24] Yadav P, Chacko S, Kumar G, Ramapanicker R, Verma V (2015) Click chemistry route to covalently link cellulose and clay, Cellulose 22 :1615-1624.

[25] Gao J, Chen J, Li X, Wang M, Zhang X, Tan F, Xu S, Liu J (2015) Azide-functionalized hollow silica nanospheres for removal of antibiotics. J. Colloid Interface Sci 444: 38–41.

[26] Nakazawa J, Smith BJ, Stack TDP (2012) Discrete complexes immobilized onto Click-SBA-15 silica: Controllable loadings and the impact of surface coverage on catalysis. J. Am. Chem. Soc 134 :2750–2759.

[27] Saad A, Vard C, Abderrabba M, Chehimi MM (2017) Triazole/Triazine-functionalized mesoporous silica as a hybrid material support for palladium nanocatalyst. Langmuir 33:7137-7146.

[28] Malvia B, Gupta SS (2012) Encapsulation of enzyme in large mesoporous material with small mesoporous window, Chem. Commun. 48 :7853-7855.

[29] Malvi B, Panda C, Dhara BB, Gupta SS (2012) One pot glucose detection by [FeIII(biuret-amide)] immobilized on mesoporous silica nanoparticles: an efficient HRP mimic. Chem. Commun. 48 :5289-5291.

[30] Tanimu A, Jillani SMS, Alluhaidan AA, Ganiyu SA, Alhooshani K (2019) 4-phenyl-1, 2, 3-triazole functionalized mesoporous silica SBA-15 as sorbent in an efficient stir bar-supported micro-solid-phase extraction strategy for highly to moderately polar phenols. *Talanta* 194:377-384.

[31] Stawicka K, Drazkiewicz K, Ziolek M *(*2018) The effect of structure of mesoporous silica and niobiosilicate on incorporation and stability of modifiers introduced by the click reaction catalyzed by different copper salts. Microporous Mesoporous Mater. *258:*41-54.

[32] Jin S, Qiao Y, Xing J (2018) Ternary mixed-mode silica sorbent of solid-phase extraction for determination of basic, neutral and acidic drugs in human serum. Anal. Bioanal. Chem. 410:3731-3742.

[33] Khaniani Y, Badiei A, Ziarani GM (2012) Application of clickable nanoporous silica surface for immobilization of ionic liquids. J. Mater. Sci. Res. 27: 932-938.

[34] Turgis R, Arrachart G, Delchet C, Rey C, Barré Y, Rostaing SP, Guari Y, Larionova J, Grandjean A (2013) An original "Click and Bind" approach for immobilizing copper hexacyanoferrate nanoparticles on mesoporous silica. Chem. Mater. 25 :447−445.

[35] Babaei Z, Chermahini AN, Dinari M, Saraji M, Shahvar A (2019) A sulfonated triazine-based covalent organic polymer supported on a mesoporous material: a new and robust material for the production of 5-hydroxymethylfurfural. Sustain. Energ Fuels 3: 1024-1032.

[36]Hosseini S.H, Zohreh N, Alipour S, Busuioc C, Negrea R (2018) Gold nanoparticles stabilized on SBA-15 functionalized NNN-pincer ligand; highly effective catalyst for reduction of nitroarenes in aqueous medium. Catal Commun. 108:93-97.

[37]Taheri R, Bahramifar N, Zarghami MR, Javadian H, Mehraban Z (2017) Nanospace engineering and functionalization of MCM-48 mesoporous silica with dendrimer amines based on [1, 3, 5]-triazines for selective and pH-independent sorption of silver ions from aqueous solution and electroplating industry wastewater. Powder Technol. 321: 44-54.

[38]Zhao D, Feng J, Huo Q, Melosh N, Fredrickson G, Chmelka B (1998) Triblock copolymer syntheses of mesoporous silica with periodic50–300 Angstrom Pores. Science. 279 :548-552.

[39] Malvi B, Sarkar BR, Pati D, Mathew R, Ajithkumar T G, Gupta SS (2009) ''Clickable'' SBA-15 mesoporous materials: synthesis, characterization and their reaction with alkynes. J. Mater. Chem.19: 1409–1416.

[40] Brunauer S, Emmett PH, Teller E (1938) Surface area measurements of activated carbons, silica gel and other adsorbents, J. Am. Chem. Soc. 60 309-319.

[41]Barrett EP, Joyner LG, Halenda PP (1951) The determination of pore volume and area distributions in porous substances. I. computations from nitrogen isotherms. J. Am. Chem. Soc. 73:373–380.

[42] Sun D, Miao X, Zhang K, Kim H, Yuan Y (2011) Triazole-forming waterborne polyurethane composites fabricated with silane coupling agent functionalized nano-silica. J. Colloid Interface Sci. 361: 483-490.

[43] Raji F, Pakizeh M (2013) Study of Hg (II) species removal from aqueous solution using hybrid $ZnCl_2$-MCM-41 adsorbent. Appl. Surf. Sci. 282:415–424.

[44] Kar M, Malvi B, Das A, Panneri S, Gupta SS (2011) Synthesis and characterization of poly-L-lysine grafted SBA-15 using NCA polymerization and click chemistry, J. Mater. Chem. 21 6690–6697.

[45] Huang D, Yang G, Feng X, Lai X, Zhao P (2015) Triazole stabilized gold and related noble metal nanoparticles for 4-nitrophenol reduction, New J. Chem. 39:4685−4694.

[46] Khalifa ME, Abdelrahman EA, Hassanien MM, Ibrahim WA (2020) Application of mesoporous silica nanoparticles modified with dibenzoylmethane as a novel composite for efficient removal of Cd (II), Hg (II), and Cu (II) ions from aqueous media. J Inorg Organomet Polym Mater 30: 2182-2196.

[47] Castle JE, Watts JF (1981) Corrosion Control by Organic Coatings, ed. H. Leidheiser, NACE, Houston: 78.

[48] Saad A, Abderrabba M, Chehimi MM (2017) X-ray induced degradation of surface bound

azido groups during XPS analysis, Surf. Interface Anal. 49 :340-344.

[49] Morère J, Tenorio MJ, Torralvo MJ, Pando C, Renuncio JAR, A. Cabanas (2011) Deposition of Pd into mesoporous silica SBA-15 using supercritical carbon dioxide. J. Supercrit. Fluids 56: 213-222.

[50] Sharma P, Singh AP (2014) Synthesis of a recyclable and efficient Pd (II) 4-(2-pyridyl)-1,2,3-triazole complex over a solid periodic mesoporous organosilica support by "click reactions" for the Stille coupling reaction, RSC Adv. 4 **:**43070-43079.

[51] Rabti A, Hannachi A, Maghraoui-Meherzi H, Raouafi N (2018) Ferrocene–functionalized carbon nanotubes: an adsorbent for Rhodamine B. Chem. Afr. 2 :1-10.

[52] Beagan A, Alotaibi K, Almakhlafi M, Algarabli W, Alajmi N, Alanazi M, Alwaalaha H, Alharbia F, Alshammaria R, Alswieleh A. (2022). Amine and Sulfonic Acid Functionalized Mesoporous Silica as an Effective Adsorbent for Removal of Methylene Blue from Contaminated Water. J King Saud Univ-Sci, 34 : 101762.

[53] Li D, Chai K, Yao X, Zhou L, Wu K, Huang Z, Yan J, Qin X, Wei W, Ji H (2021) β-Cyclodextrin functionalized SBA-15 via amide linkage as a super adsorbent for rapid removal of methyl blue. J. Colloid Interface Sci. 583: 100-112.

[54] Dong Y, Lu B, Zang S, Zhao J, Wang X, Cai Q (2011) Removal of methylene blue from coloured effluents by adsorption onto SBA- 15, J. Chem. Technol. Biotechnol. 86: 616-619

[55] Cherifi Z, Boukoussa B, Mokhtar A, Hachemaoui M, Zeggai FZ, Zaoui A, Bachari K, Meghabar R (2020) Preparation of new nanocomposite poly (GDMA)/mesoporous silica and its adsorption behavior towards cationic dye. React Funct Polym 153: 104611

[56] Liang Z, Zhao Z, Sun T, Shi W, Cui F (2017). Enhanced adsorption of the cationic dyes in the spherical CuO/meso-silica nano composite and impact of solution chemistry. J Colloid Interface Sci 485:192-200.

[57] Chen Q, He Q, Lv M, Xu Y, Yang H, Liu X, Wei F (2015) Selective adsorption of cationic dyes by UiO-66-NH_2, Appl. Surf. Sci.327: 77-85.

[58] Zhang J, Li F, Sun Q (2018) Rapid and selective adsorption of cationic dyes by a unique metal-organic framework with decorated pore surface. Appl. Surf. Sci. 440 :1219-1226.